Available online at www.sciencedirect.com
ScienceDirect
Journal of Nuclear Materials 373 (2008) 415–423
journal of nuclear materials
www.elsevier.com/locate/jnucmat

Ductile-to-brittle transition of oxidised Zircaloy-4 and E110 claddings

Zoltán Hózer [a,*], Csaba Győri [b], Lajos Matus [a], Márta Horváth [a]

[a] Hungarian Academy of Sciences, KFKI Atomic Energy Research Institute, P.O. Box 49, H-1525 Budapest, Hungary
[b] European Commission, Joint Research Centre, Institute for Transuranium Elements, P.O. Box 2340, D-76125 Karlsruhe, Germany

Received 8 January 2007; accepted 10 July 2007

Abstract

The ductile-to-brittle transition of the claddings of PWR and VVER nuclear fuel rods has been investigated in ring compression tests performed at room temperature with Zircaloy-4 and E110 samples oxidised in high temperature steam. These experiments were evaluated on the basis of the form of load–displacement curves. The ductile samples were characterised by a horizontal ductile plateau after the elastic deformation, while in the case of the brittle samples the ductile plateau was missing. The ductility limits of both alloys were expressed in terms of oxidation time and cladding temperature. From this, a numerical procedure was derived for the simulation of Zr cladding embrittlement during loss-of-coolant accidents. The results indicated a faster embrittlement of the E110 alloy than that of the Zircaloy-4 under identical conditions. The new approach is proposed as an alternative of the 17% ECR criterion to evaluate cladding embrittlement in design basis accident (DBA) scenarios.

PACS: 28.52.Nh

1. Introduction

During a loss-of-coolant accident (LOCA) the fuel rods in a nuclear reactor overheat and the coolant pressure drops to a low value. These effects can lead to mechanical, structural and chemical changes in the zirconium claddings used in most of the nuclear power plants. The fuel rod integrity can be lost in two ways during the high temperature LOCA scenario:

- Ductile failure is typical at the beginning of the accident right after the blow-down. The cladding becomes plastic when its temperature has exceeded ≈800 °C and can balloon due to the pressure difference between the inside and outside of the fuel rod. A ballooned rod segment bursts when the local strain and stress reach critical values. The main consequences of the ballooning and the subsequent burst are the release of radioactive materials from the failed fuel rods and the reduction of the flow cross-section in the fuel assembly. The blockage formation can lead to 70–80% reduction of the flow cross-section, but even in this case the core remains coolable [1,2].
- Brittle failure can be expected after several minutes of high-temperature oxidation in steam, at the late phase of the accident, when the hot fuel rods are quenched by cold water. The thermal and mechanical loads can lead to the formation and propagation of cracks in the brittle cladding and, finally, to the fragmentation of the fuel rod. In this case the final arrangement of the fuel rod fragments cannot be predicted due to the large variety of potential configurations and, for this reason, the coolability is uncertain.

Since the coolability of the reactor core must be maintained to prevent severe fuel rod degradation, the brittle failure of the fuel rods should be avoided if at all possible. Therefore, the zirconium alloys must keep some ductile behaviour during a LOCA accident. The embrittlement of the zirconium alloys under high temperature conditions is caused by the oxidation and the accompanying hydrogen absorption. Limiting the degree of oxidation, i.e. the time

* Corresponding author. Tel.: +36 1 3922294; fax: +36 1 3959293.
E-mail address: Hozer@sunserv.kfki.hu (Z. Hózer).

0022-3115/$ - see front matter © 2007 Elsevier B.V. All rights reserved.
doi:10.1016/j.jnucmat.2007.07.002

and/or temperature of the $Zr + 2H_2O \rightarrow ZrO_2 + 2H_2$ reaction, in turn limits the cladding embrittlement, thus fuel rod fragmentation can be avoided and the coolable core geometry can be guaranteed.

LOCA-related fuel safety criteria today limit the peak cladding temperature (PCT) and the degree of oxidation in terms of 'equivalent cladding reacted' (ECR). These criteria were first accepted in the US in 1973 [3] and the threshold values of 1200 °C PCT and 17% ECR were determined. The establishment of these criteria was based on ring compression tests of oxidised Zircaloy-4 cladding at 135 °C [4]. Later similar LOCA criteria were introduced in many other countries with similar ECR values for different Zr alloys. Thermal shock tests simulating the integral behaviour of fuel rods during postulated LOCA conditions were also performed to confirm the correctness of the criteria [5–7].

However, during the evaluation of thermal shock test results, the ECR is usually not a measured parameter, but is calculated supposing two-sided oxidation and applying a conservative oxidation kinetics correlation. As the inner side of the cladding cannot be oxidised as intensively as the outer surface if the oxidation follows realistic kinetics, so that the ECR determined in this manner will be much higher than the real degree of oxidation. Furthermore, the identification of intact and failed specimens is not exact: in some cases a small crack in the cladding is considered as failure indicator, in other cases additional mechanical tests are carried out with oxidised and quenched samples to determine the degree of their embrittlement. These uncertainties explain how the same ECR limit that was originally conceived for Zircaloy-4 at 135 °C in Hobson's ring compression tests [4] could be derived for different alloys at room temperature [5,7].

The radiation and the high neutron fluence in the nuclear reactors lead to the embrittlement of the reactor pressure vessel. This process can endanger the integrity of the vessel wall in accidents with pressurised thermal shock (PTS) conditions. The surveillance programmes tracking the change of mechanical properties include only standard mechanical testing (the well known Charpy tests) and do not try to simulate PTS conditions [8,9]. The Charpy impact test provides a reliable and low-cost method with high accuracy and reproducibility. Therefore it is widely used as standard test method in different industrial and scientific applications [10,11].

The introduction of new cladding materials for the fuel rods of nuclear reactors should also demand a standard method for the evaluation of ductile-to-brittle transition under LOCA conditions. The more so, as several experiments have indicated significant differences in the oxidation kinetics and the mechanical behaviour between different Zr alloys at high temperature [12–14]. For this reason specific LOCA criteria should be identified for each cladding material. The use of standard testing procedures – similarly to the investigation of reactor vessel embrittlement – should facilitate the comparison of different alloys and the establishment of alloy-specific fuel safety criteria. A potential candidate for standard testing could be the ring compression test technique using standard tensile test machines. This procedure is commonly used in different laboratories for the investigation of oxidised Zr claddings [4,7,12–16].

2. Experiments

2.1. Sample preparation

The embrittlement process of E110 and Zircaloy-4 cladding specimens was investigated at different corrosion states. The E110 tube of VVER fuels was received from Russia, while the Zircaloy-4 cladding used in PWRs was of German origin. The two claddings were produced with different alloying elements and using different technologies. The main components of Zircaloy-4 were 1.5 wt% Sn, 0.2 wt% Fe, 0.1 wt% Cr and 0.1 wt% O. The E110 alloy consisted of 1.0 wt% Nb, 0.05 wt% O, 0.01 wt% Fe and 0.01 wt% Hf. The samples were cut from cladding tubes without pellets. The diameter and the wall thickness of the tubes were 9.1/0.65 mm for E110 and 10.75/0.625 for Zircaloy-4. The samples were uniformly 8 mm long. For both types of alloys the same experimental procedures and equipment were applied in order to avoid any system effect. The surfaces were degreased before the experimental procedures. Then the initial weight and size of the samples were measured to an accuracy of 0.01 mg and 0.01 mm, respectively. The samples were tested without end-plugs so that double-sided oxidation would occur.

2.2. Oxidation

The oxidation of the specimens was performed in steam and argon mixture including 12 vol.% argon gas. This small amount of inert gas does not influence the oxidation kinetics but, as a carrier gas, enhances the accuracy of the hydrogen concentration measurement during the reaction. The inlet gas velocity was 8.5–11 cm/s, which meant unlimited steam supply for the oxidation. The oxidation temperature was varied between 900 °C and 1200 °C in steps of 100 °C and the samples were oxidised at each temperature for times varying between 10 s and 11 400 s. In all cases the oxidation was measured on both internal and external surfaces of the cladding. Detailed information on the oxidation conditions of the Zircaloy-4 and E110 samples are presented in Tables 1 and 2, respectively.

After heating up the tube furnace to the required temperature and adjusting the constant gas flow through the system, the sample was moved into the hot zone of the furnace and was exposed to steam oxidation under isothermal conditions. The sample was withdrawn from the hot zone of the furnace after the required oxidation time. During oxidation the hydrogen concentration in the outlet gas flow was monitored on-line. The time-history of the hydrogen production showed the intensity of the oxidation and its integral gave a first estimation of the hydrogen fraction absorbed by the zirconium alloy.

Table 1
Main characteristics of Zircaloy-4 samples

Sample	Oxidation temperature (°C)	Oxidation time (s)	Measured equivalent cladding reacted (%)	Hydrogen content (ppm)	Specific energy at failure (J/m)	Ductile or brittle
Y-11	900	300	2.28	3	412.64	Ductile
Y-10	900	1000	3.49	2	318.66	Ductile
Y-8	900	5000	5.93	2	104.61	Ductile
Y-9	900	11000	7	1	83.71	Ductile
Y-6	1000	87	2.89	1	333.23	Ductile
Y-5	1000	464	6.02	1	126.74	Ductile
Y-1	1000	2600	12.26	1	37.78	Brittle
Y-7	1000	3300	15.18	8	22.46	Brittle
Y-4	1000	4090	20.37	997	9.21	Brittle
Y-3	1000	7270	44.03	1854	2.19	Brittle
Y-2	1000	11360	77.29	110	0.36	Brittle
Y-17	1100	27	2.83	1	431.51	Ductile
Y-16	1100	102	5.45	1	343.06	Ductile
Y-15	1100	398	10.11	3	147.41	Ductile
Y-14	1100	900	15.21	2	47.81	Brittle
Y-13	1100	1500	19.49	2	22.98	Brittle
Y-12	1100	3000	26.77	5	9.03	Brittle
Y-23	1200	10	3.48	1	309.14	Ductile
Y-22	1200	40	5.76	1	130.54	Ductile
Y-21	1200	163	10.48	1	39.18	Brittle
Y-20	1200	367	15.36	1	14.89	Brittle
Y-18	1200	790	21.85	5	9.01	Brittle
Y-19	1200	1100	25.73	1	5.46	Brittle

Table 2
Main characteristics of E110 samples

Sample	Oxidation temperature (°C)	Oxidation time (s)	Measured equivalent cladding reacted (%)	Hydrogen content (ppm)	Specific energy at failure (J/m)	Ductile or brittle
N-14	900	350	1.62	8	470.26	Ductile
N-13	900	1000	3.69	356	88.90	Ductile
N-11	900	3000	8.63	1325	8.86	Brittle
N-12	900	7000	13.76	2359	2.05	Brittle
N-10	900	11000	18.86	2896	1.90	Brittle
N-9	900	14000	19.32	2630	1.46	Brittle
N-7	1000	100	1.94	1	438.23	Ductile
N-2	1000	700	6.2	908	11.61	Brittle
N-6	1000	1200	9.47	1812	6.01	Brittle
N-5	1000	1800	16.95	3135	1.51	Brittle
N-3	1000	3600	23.72	3274	0.91	Brittle
N-1	1000	6000	30.23	2330	0.76	Brittle
N-19	1100	19	1.57	18	411.78	Ductile
N-18	1100	133	4.72	598	10.00	Brittle
N-17	1100	704	11.42	907	5.44	Brittle
N-16	1100	1500	16.82	679	4.48	Brittle
N-15	1100	2400	21.78	704	2.71	Brittle
N-8	1100	5000	31.47	920	0.42	Brittle
N-25	1200	7	2.19	4	322.86	Ductile
N-24	1200	49	4.93	11	52.51	Ductile
N-23	1200	167	10.16	786	5.48	Brittle
N-22	1200	380	14.76	611	5.18	Brittle
N-21	1200	646	19.35	550	3.44	Brittle
N-20	1200	1205	26.58	580	1.46	Brittle

2.3. Mechanical tests

Ring compression tests were applied to determine the change of cladding ductility and to characterize the embrittlement process as a function of the oxidation time and temperature. The as-received and pre-oxidised ring specimens were examined in radial compression tests using an Instron 1195 universal test machine. The velocity of the crosshead movement was fixed at 2 mm/min. All tests were performed at room temperature.

The load versus crosshead displacement curves were recorded and the crushing force and deformation were

determined. Generally 2–3 cracks were detected but always the first crack was considered as the sign of failure. The rings were compressed until total plastic deformation had occurred or at least until the first indication of cracking. The load–displacement curves were evaluated to characterize the mechanical behaviour of the samples.

2.4. Post-test examinations

The samples were reweighed before mechanical testing (accuracy: ±0.01 mg). The weight gains were used to determine the amount of oxygen taken during the oxidation (the correction for the weight of absorbed H_2 contained in the remaining metallic phase was made using the values of absorbed H_2 determined by hot extraction – see below). The degree of oxidation (ECR) was defined as the ratio of the amount of oxygen taken up by the sample and the amount of oxygen corresponding to the full oxidation of the specimen (0% for the initial state and 100% for total oxidation). The ECR values are listed in column 4 of Tables 1 and 2.

The accurate hydrogen content of the samples was determined after the mechanical tests by the high-temperature desorption method (see column 5 of Tables 1 and 2). This procedure requires small pieces of the rings that can be produced only with destructive methods. Since the hydrogen content does not change during ring compression tests at room temperature, it was expedient to carry out sampling for hydrogen desorption after mechanical testing.

The metallographic analysis of the tested sample cross-sections was carried out with a Reichert Me-F2 optical microscope to verify the extent of oxidation and the form and porosity of the oxide layers.

3. Results and discussion

3.1. Oxidation of Zircaloy-4 and E110 claddings in steam

The oxidation behaviour of E110 and Zircaloy-4 was similar both at 1100 °C and 1200 °C, while at lower temperatures the oxidation rate was higher for E110 (Fig. 1). The oxidation results were in good agreement with the existing steam oxidation correlations for E110 [15] and Zircaloy-4 [17] and with our earlier studies [18] as well.

The metallographic observation of the samples revealed that the morphology of oxide layers was different on the two alloys. For Zircaloy-4 the oxide layer in most of the cases was compact, for the E110 alloy the typical picture showed a layered structure and the breakaway effect.

The oxide layer structure of four different samples are presented in Figs. 2(a)–(d). The E110 samples oxidised at 1000 °C had an oxide scale with a layered structure (Fig. 2(a)) The oxide scale was more compact at 1200 °C, but many radial cracks were observed, which may have facilitated the penetration of hydrogen into the metal (Fig. 2(b)). In the case of Zircaloy-4 the oxide layer was

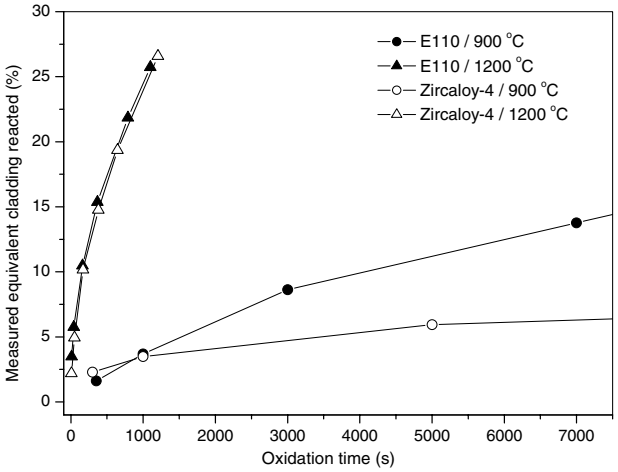

Fig. 1. Oxidation of E110 and Zircaloy-4 at 900 °C and 1200 °C.

Fig. 2(a). Cross-section of E110 cladding oxidised at 1000 °C (sample N-3).

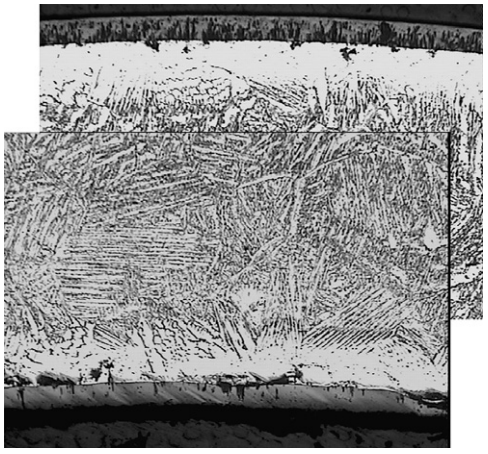

Fig. 2(b). Cross-section of E110 cladding oxidised at 1200 °C (sample N-22).

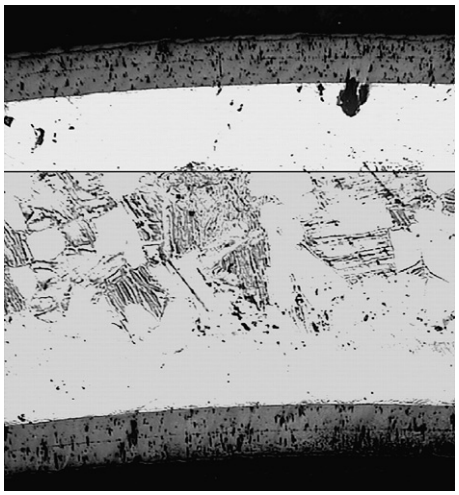

Fig. 2(c). Cross-section of Zircaloy-4 cladding oxidised at 1200 °C (sample Y-19).

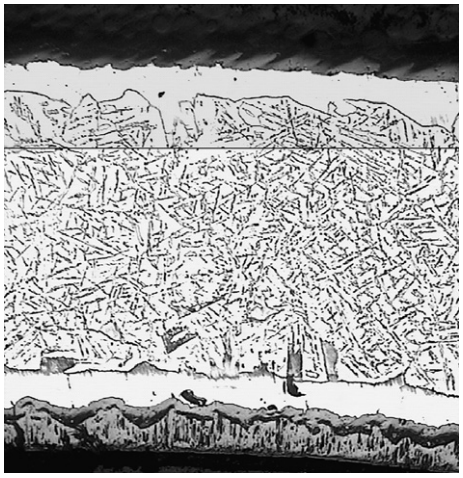

Fig. 2(d). Cross-section of Zircaloy-4 cladding oxidised at 1000 °C (sample Y-4).

compact at 1200 °C (Fig. 2(c)), but the oxide scale formed at 1000 °C indicated breakaway phenomena (Fig. 2(d)).

3.2. Hydrogen uptake

The measurements of the hydrogen content indicated very low hydrogen uptake by Zircaloy-4 at temperatures below and above 1000 °C (Fig. 3). But, by contrast, the samples oxidised at 1000 °C contained up to 1800 ppm hydrogen. This high value is obviously the consequence of the breakaway effect, which allowed the produced hydrogen to reach the metallic surfaces through the cracks in the oxide layer. One sample with very long oxidation time (Y-2 in Table 1) showed a low hydrogen content, because the residual metallic part became very thin and the gas absorbed earlier was released during the late phase of oxidation.

The E110 specimens absorbed much more hydrogen than the Zircaloy-4 ones (Fig. 3). At 900 °C and 1000 °C,

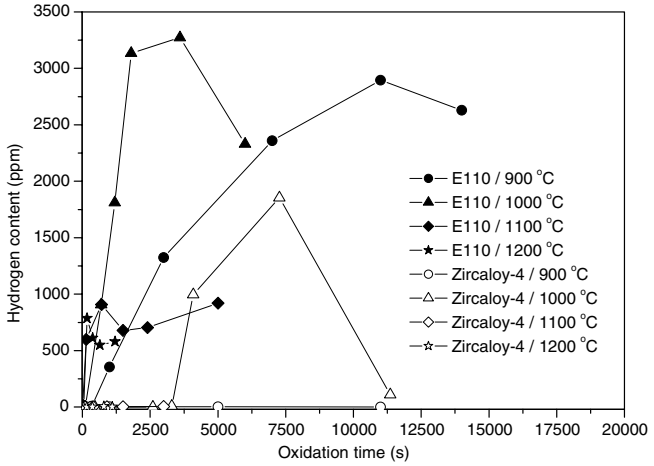

Fig. 3. Hydrogen content of E110 and Zircaloy-4 oxidised in steam atmosphere between 900 °C and 1200 °C.

the hydrogen content reached the values of 2000–3000 ppm in 1–2 h oxidation time. The typical degree of oxidation (measured ECR) for those samples was about 20%. The hydrogen content was maximum 800–900 ppm at higher temperatures (1100 °C and 1200 °C) reached within 3–10 min at about 10% ECR. In the case of low oxidation the hydrogen content was negligible even in the E110 samples, because the cracking of the oxide layer started only above 8–14 m oxide scale thickness and the initial compact layer was able to prevent the access of hydrogen to the metallic surface.

The β-phase zirconium in E110 samples with high hydrogen content had a needle-shaped structure. Figs. 2(a) and 2(b) show the structure of samples with 600 ppm and 3000 ppm hydrogen contents, respectively. The pictures indicate that the higher hydrogen content resulted in a finer structure. The Zircaloy-4 samples with very low hydrogen content did not show a structure like that in the phase (Fig. 2(c)). The Zircaloy-4 samples with high hydrogen content had a needle-shaped phase as well (Fig. 2(d)), but their structure was not as fine as in the E110 samples with similar hydrogen content. Hydrides cannot be observed in these samples, since the hydrogen uptake took place at high temperature and the hydrogen was dissolved in the metallic phase without formation of hydride grains.

3.3. Mechanical performance of oxidised Zircaloy-4 and E110 claddings

The as-received (non-oxidised) samples were completely plastic, they deformed without cracking in the ring compression test. The samples containing oxygen and hydrogen in a significant amount exhibited a more brittle behaviour. Fig. 4 shows five load–displacement curves recorded during the ring compression tests of E110 specimens oxidised at 1000 °C. The curves start with a slope indicating elastic deformation. The top curve – representing a sample with

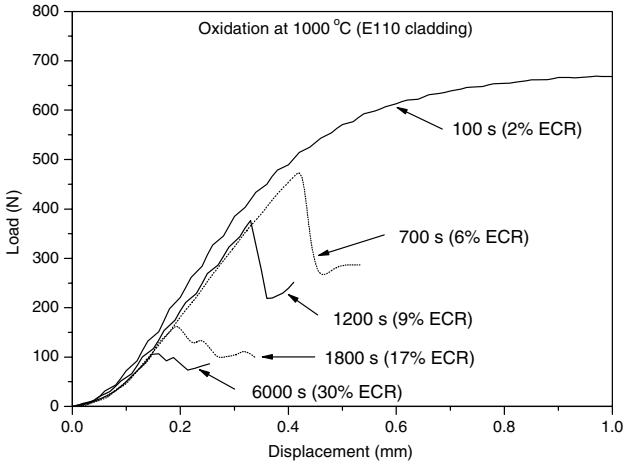

Fig. 4. Force–displacement diagrams recorded during radial ring compression testing of E110 samples oxidised in steam.

low oxidation (2% ECR) – continues in a horizontal ductile plateau indicating plastic deformation. The other four curves break down after the elastic slope at different loads. The curves clearly show that the more oxidised samples can withstand less mechanical load.

Analysing the load–displacement curves several parameters can be derived, e.g., maximum load, maximum deformation (displacement at failure), relative total deformation, residual ductility, and energy at failure. Fig. 5 represents a typical load–displacement curve indicating the above parameters. The failure of the ring is presumed to occur at the point of maximum load and the parameters are determined using this point of the curve. The residual ductility corresponds to a relative plastic deformation: this is the plastic displacement at maximum load indicated in the figure divided by the outer diameter of the specimen. Correspondingly, the relative total deformation is the total displacement (at maximum load) divided by the specimen diameter. The specific energy at failure is determined as the total deformation energy at failure divided by the length of the ring. With this last parameter the results of different laboratories with different ring lengths can be compared.

The relative total deformation, the residual ductility and the specific energy at failure are not independent of each other. The relative total deformation and the residual ductility depend linearly on the specific energy at failure, and have the same slope (see Fig. 6). However, the values of the relative total deformation are ≈5% higher than those of the residual ductility, since the total displacement includes the elastic deformation as well.

3.4. Ductile-to-brittle transition

On the basis of the load–displacement curves of the ring compression tests the ductile or brittle character of the cladding specimens can be determined. The load–displacement curves of some E110 samples tested in the present series are shown in Fig. 4. One can distinguish between two types of curves:

- *Ductile* curves are characterised by a horizontal ductile plateau after the elastic deformation (upper curve in Fig. 4).
- In the case of *brittle* curves the ductile plateau is missing, and the elastic deformation is followed by a quick breakdown indicating the formation of cracks and the rupture of the sample.

The Zircaloy-4 samples displayed a similar division in the curves. It must be noted that similar behaviour can be observed in other mechanical tests such as ring tensile and three-point bend.

The categorisation of the specimens to 'ductile' or 'brittle' could have been performed on the basis of the parameters listed in the previous section. Generally the residual ductility is used to characterise the specimens with the limit

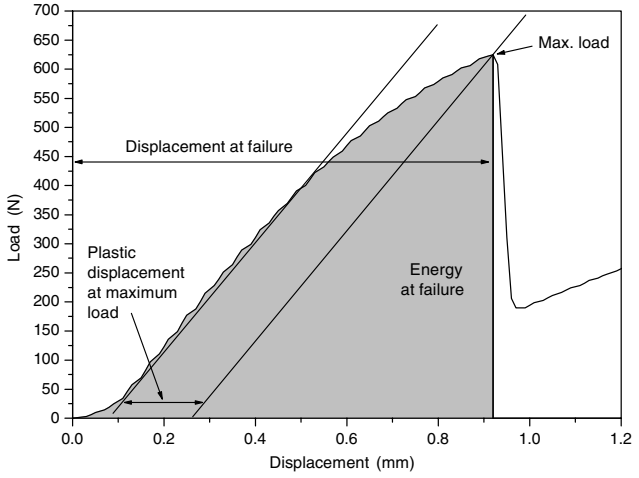

Fig. 5. Determination of failure characteristics on the basis of load–displacement curve.

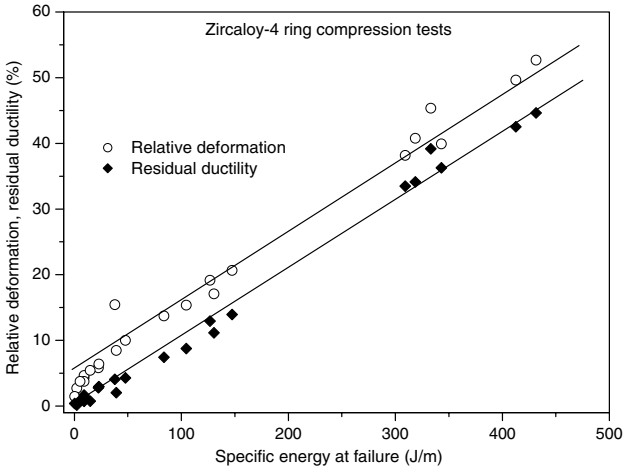

Fig. 6. Relative deformation and residual ductility as a function of the specific energy at failure for Zircaloy-4 samples.

value of 1–2% for the ductile-to-brittle transition. However, the derivation of the residual ductility involves several uncertainties concerning the selection of the elastic deformation region in the recorded diagram. Another possibility is to separate the ductile and brittle specimens on the basis of the specific energy at failure. This parameter can be easily defined through the integration of the load–displacement curve up to the first indication of cracking. After the analyses of the load–displacement curves recorded in the tests of the E110 and Zircaloy-4 specimens a clear limit of 50 J/m was derived for the ductile-to-brittle transition of both claddings. (Thus Tables 1 and 2 indicate that the ductile samples had the specific energy at failure above 50 J/m for both Zircaloy-4 and E110 alloys, while for the brittle samples the first crack appeared below 50 J/m.) Following the methodology proposed by Vitanza [19] and representing the time of oxidation for each specimen versus the reciprocal oxidation temperature, we could determine the ductile-to-brittle transition (or with other words the ductility limit) separately for E110 and Zircaloy-4, as indicated in Figs. 7 and 8. The ductile and brittle specimens are indicated with different markers in both figures. A line, representing the ductility limit, was drawn to separate the points in a conservative way: all the 'brittle' points and a few 'ductile' points are above the line, and the remaining 'ductile' points are below the line. This approach guarantees that the cladding has some ductility under the oxidation conditions below the line.

The ductile-to-brittle transition curves determine an exponential relationship between the critical oxidation time and temperature. If the oxidation time is shorter at a given temperature than the limiting value (t^*), the cladding will still be ductile after the oxidation. The expressions have the following forms:

$$\text{E110:}\quad t^* = 2\times 10^{-4}\mathrm{e}^{17500/T}, \tag{1}$$

$$\text{Zircaloy-4:}\quad t^* = 10^{-4}\mathrm{e}^{20000/T}, \tag{2}$$

where

t^* – time of oxidation to reach ductile-to-brittle transition limit (s),
T – cladding temperature (K).

Note that the above expressions describe the ductile-to-brittle transition of Zr claddings at room temperature after double-sided oxidation in steam.

Similarly to the results of earlier work performed by Böhmert et al. [12], the ring compression tests in the present work showed a different mechanical behaviour of the two alloys. Comparing Figs. 7 and 8 it becomes obvious that the ductile-to-brittle transition of the E110 cladding takes places earlier (i.e. at lower oxidation temperature or shorter oxidation time) than that of the Zircaloy-4 cladding. The ductility limit curves are compared in Fig. 9 as well, indicating an approximately 100 K shift between the two alloys for the same oxidation time. Accordingly, the Zircaloy-4 cladding can be oxidised at a higher temperature for the same period than the E110 tubes to reach the ductile-to-brittle transition.

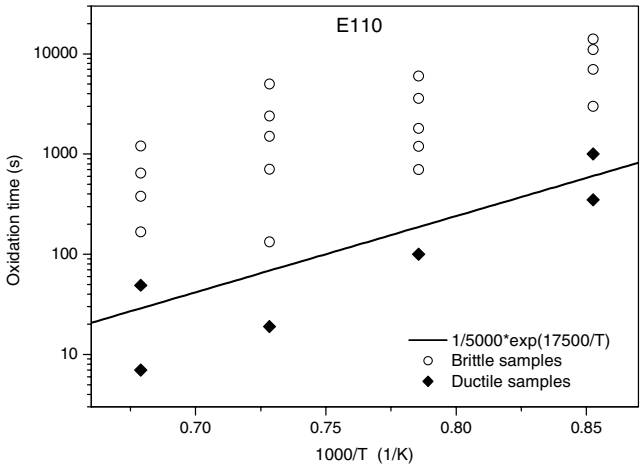

Fig. 7. Ductile and brittle oxidised E110 samples.

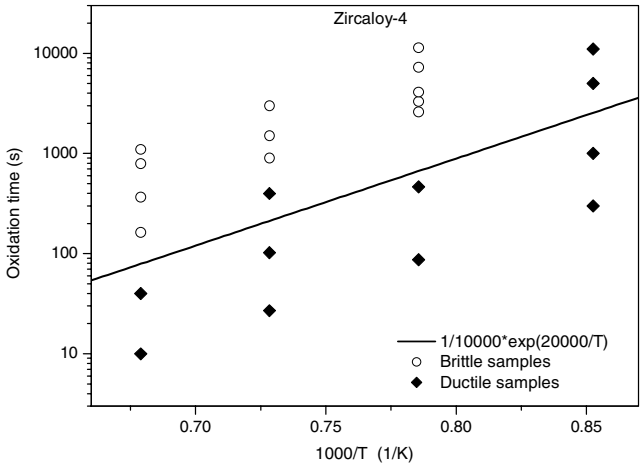

Fig. 8. Ductile and brittle oxidised Zircaloy-4 samples.

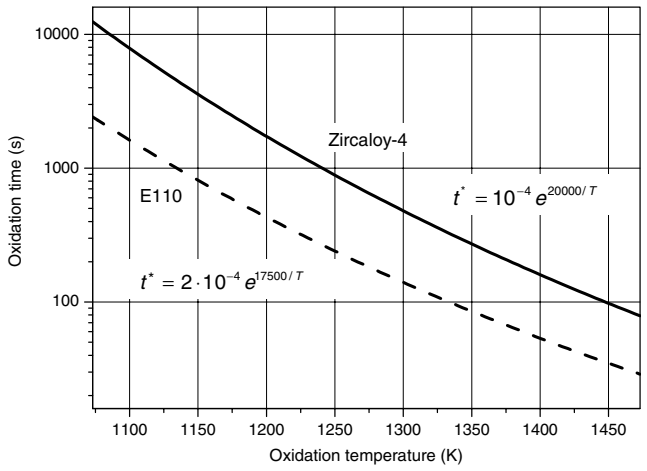

Fig. 9. Ductile-to-brittle transition functions for Zircaloy-4 and E110 claddings.

Let us emphasize that the ductile-to-brittle transition is generally used to characterise material properties. In the zirconium oxidation case the oxide layer properties of the tubular cladding cannot be transferred to another geometry or sample thickness. For this reason the evaluated expressions can be used for the investigated geometry only. However, the fuel cladding geometry (diameter and wall thickness) does not differ too much for the different reactors, and so the ductile-to-brittle transition described here can be considered as a general characteristic for Zircaloy-4 and E110 type claddings.

3.5. Calculation of the ductile-to-brittle transition in transient conditions

The ductility limits presented in terms of time in the previous chapter concern only isothermal conditions and cannot be applied directly in the safety analyses of design basis accidents (DBA). However, a method to calculate the ductile-to-brittle transition of Zr claddings in transient conditions can facilitate the evaluation of cladding ductility after LOCA accidents. Assuming that the embrittlement of the cladding as a function of time is closely related to the oxidation process, a simple approach is proposed here.

The ductility limit (time of oxidation resulting in the loss of ductility) is presented as a function of temperature by the following relationship:

$$t^* = A\mathrm{e}^{B/T}, \tag{3}$$

where A and B are cladding-specific coefficients given in Eqs. (1) and (2) for E110 and Zircaloy-4 alloys.

Considering that the kinetics of the cladding oxidation under isothermal conditions follows a parabolic rule we can introduce an appropriate ductility parameter P as a function of time and temperature using Eq. (3):

$$P = \sqrt{\frac{t}{A\mathrm{e}^{B/T}}}. \tag{4}$$

This parameter represents the square root of a relative time (actual oxidation time/ductility limit), meaning that under isothermal steam oxidation the cladding remains ductile if $P < 1$, and becomes brittle if $P \geqslant 1$.

For transient conditions in a LOCA case the ductility parameter P can be calculated by means of a quasi-stationary approach on the analogy of the ZrO_2 layer growth:

$$P_i = \sqrt{P_{i-1}^2 + \frac{\Delta t}{A\mathrm{e}^{B/T}}}, \tag{5}$$

where

P_i – ductility parameter in the actual time step,
P_{i-1} – ductility parameter in the previous time step,
Δt – time step while the temperature is assumed constant.

In this manner the ductility parameter can be calculated step by step in time on the basis of the local cladding temperature either simultaneously with or after a thermohydraulic analysis of the postulated accident. Thus the above simple algorithm provides an easy evaluation of the cladding ductility on the basis of the calculated temperature history in a LOCA, independently of any oxidation model. If the value of P calculated from the accident initiation to the time point of the quenching is below 1 than the cladding ductility will be sufficient to maintain fuel rod integrity following the thermal shock.

4. Conclusions

The ductile-to-brittle transition of Zircaloy-4 and E110 (Zr1%Nb) claddings due to high temperature oxidation in steam was investigated through ring compression tests of pre-oxidised specimens. Different embrittlement behaviour of these two alloys was observed and explained by the considerably higher hydrogen uptake of the E110 alloy than that of Zircaloy-4. The ductility of the claddings was evaluated on the basis of the load–displacement curves. The ductile samples were characterised by a horizontal ductile plateau after the elastic deformation, while in the case of brittle samples the ductile plateau was missing. The ductile-to-brittle transition was associated with a specific energy value of 50 J/m for both alloys ($E > 50$ J/m – 'ductile' failure, $E \leqslant 50$ J/m – 'brittle' failure). In view of this value, ductility limits were determined for the two alloys as a function of the oxidation temperature. The results indicated a faster embrittlement of the E110 alloy than that of Zircaloy-4 under identical conditions. However, the safety assessment of the nuclear fuel rods in DBA cases demands a complex evaluation, considering the reactor-specific temperature history during the accident – defined by system-level thermohydraulic analyses – and the cladding corrosion under normal operation as well.

A new procedure was introduced for the evaluation of the cladding ductility under postulated LOCA conditions. The methodology is based on the computation of an appropriate ductility parameter using only a local cladding temperature. The approach makes the prediction of cladding embrittlement during DBA scenarios possible and it is proposed as an alternative of the 17% ECR criterion.

References

[1] Z. Hózer, Cs. Győri, M. Horváth, I. Nagy, L. Maróti, L. Matus, P. Windberg, J. Frecska, Nucl. Technol. 152 (2005) 273.
[2] F.J. Erbacher, Nucl. Eng. Des. 103 (1987) 55.
[3] G. Hache, H.M. Chung, in: NUREG/CP-0172, 2001, p. 205.
[4] D.O. Hobson, in: Proceedings of the ANS Topical Meeting on Water Reactor Safety, Salt Lake City, 1973, p. 274.
[5] Yu.K. Bibilashvili, N.B. Sokolov, L.N. Andreeva-Andrievskaya, V.Yu. Tonkov, A.V. Salatov, A.M. Morosov, V.P. Smirnov, in: IAEA-TECDOC-1320, International Atomic Energy Agency, 2002, p. 186.
[6] F. Nagase, M. Tanimoto, H. Uetsuka, in: IAEA-TECDOC-1320, International Atomic Energy Agency, 2002, p. 270.
[7] J.H. Kim, M.H. Lee, B.K. Choi, Y.H. Jeong, Nucl. Eng. Des. 235 (2005) 67–75.

[8] M. Valo, K. Wallin, E. Lucon, M. Kytka, M. Brumovsky, B. Acosta, L. Debarberis, J. Kohopaa, F. Gillemot, M. Horváth, Nucl. Eng. Des. 235 (2005) 445.
[9] A. Ballesteros, J. Bros, L. Debarberis, F. Sevini, D. Erak, S. Gezashchenko, A. Kryukov, Y. Shtrombakh, S. Goloshapov, A. Ionov, Y. Anikeev, G. Banyuk, A. Plusch, F. Gillemot, L. Tatar, V. Petrosyan, Nucl. Eng. Des. 235 (2005) 411.
[10] Y.J. Chao, J.D. Ward Jr., R.G. Sands, Mater. Des. 28 (2007) 551.
[11] E. Bayraktar, D. Hugele, J.P. Jansen, D. Kaplan, Mater. Proc. Technol. 147 (2004) 155–162.
[12] J. Böhmert, M. Dietrich, J. Linek, Nucl. Eng. Des. 147 (1993) 53.
[13] Z. Hózer, L. Matus, M. Horváth, L. Vasáros, Á. Griger, L. Maróti, Ring compression tests with oxidised and hydrided Zr1%Nb and Zircaloy-4 claddings, KFKI-2002-01/G KFKI, Atomic Energy Research Institute, 2002.
[14] L. Yegorova, K. Lioutov, N. Jouravkova, A. Konobeev, V. Smirnov, V. Chesanov, A. Goryachev, US Nuclear Regulatory Commission, Experimental Study of Embrittlement of Zr-1%Nb VVER Cladding under LOCA-Relevant Conditions, NUREG/IA-0211, 2005.
[15] I. Solyany, Yu. K. Bibliashvili, V.V. Dranenko, A.Ya. Levin, L.B. Izraljevskij, A.M. Morozov, in: IAEA-IWGFPT/19, International Atomic Energy Agency, 1984.
[16] V. Vrtilkova, L. Novotny, V. Hamouz, R. Doucha, I. Tinka, J. Macek, F. Lahovsky, in: Proceedings of the International Conference on Nuclear Energy for New Europe, Bled, Slovenia, 2005, Paper No. 49.
[17] S. Leistikow, G. Schanz, Nucl. Eng. Des. 103 (1987) 65.
[18] J. Frecska, G. Konczos, L. Maróti, L. Matus, Oxidation and hydriding of Zr1%Nb alloy by steam, KFKI-1995-17/G, KFKI Atomic Energy Research Institute, 1995.
[19] C. Vitanza, Discussion on experimental methods to derive LOCA safety limits, in: IAEA-TECDOC-1320, International Atomic Energy Agency, 2002, p. 224.